SCIENTIFIC REPORTS

OPEN

SUBJECT AREAS:
SOLAR CELLS
INFRARED SPECTROSCOPY
SOLAR ENERGY AND PHOTOVOLTAIC TECHNOLOGY
QUANTUM DOTS

Received
3 June 2013

Accepted
25 October 2013

Published
13 November 2013

Correspondence and requests for materials should be addressed to Y.H.L. (leeyoung@skku.edu) or H.Y.C. (hychoi@yonsei.ac.kr)

Ultrafast biexciton spectroscopy in semiconductor quantum dots: evidence for early emergence of multiple-exciton generation

Younghwan Choi[1], Sangwan Sim[1], Seong Chu Lim[2,3], Young Hee Lee[2,3] & Hyunyong Choi[1]

[1]School of Electrical and Electronic Engineering, Yonsei University, Seoul 120-749, Republic of Korea, [2]IBS Center for Integrated Nanostructure Physics, Institute for Basic Science (IBS), Daejon 305-701, Republic of Korea, [3]Department of Energy Science, Sungkyunkwan University, Suwon, 440-746, Republic of Korea.

Understanding multiple-exciton generation (MEG) in quantum dots (QDs) requires in-depth measurements of transient exciton dynamics. Because MEG typically faces competing ultrafast energy-loss intra-band relaxation, it is of central importance to investigate the emerging time-scale of the MEG kinetics. Here, we present ultrafast spectroscopic measurements of the MEG in PbS QDs via probing the ground-state biexciton transients. Specifically, we directly compare the biexciton spectra with the single-exciton ones before and after the intra-band relaxation. Early emergence of MEG is evidenced by observing transient Stark shift and quasi-instantaneous linewidth broadening, both of which take place before the intra-band relaxation. Photon-density-dependent study shows that the broadened biexciton linewidth strongly depends on the MEG-induced extra-exciton generation. Long after the intra-band relaxation, the biexciton broadening is small and the single-exciton state filling is dominant.

The limiting factor for improving solar-cell efficiency lies in the simple physics that single-photon absorption generates one electron-hole pair[1]. The possibility of generating multiple charge carriers per photon, known as carrier multiplication (CM) or multiple exciton generation (MEG), is of crucial importance for developing efficient solar-cell devices[2–8]. Semiconductor quantum dots (QDs) represent well-defined structures to explore the quantum limit of harnessing solar-conversion efficiency[9–13]. By engineering the sizes of QD composites, it has been demonstrated that not only the optical properties[14,15], but also the MEG efficiency in QDs can be modified[16]. MEG in a photo-excited QD system is a prominent route for enhancing the conversion efficiency because carriers confined in spatial dimensions that are smaller than the bulk exciton Bohr radius lead to the formation of discrete excitonic states such that efficient MEG is possible either by suppressing the ultrafast electron-phonon relaxation[4,17,18] or by enhancing the Coulomb interactions via reduced dielectric screening at the QD surface[19].

Numerous investigations have shown that the kinetic origin of MEG dynamics in QDs is intrinsically complex because the photo-generated single exciton initially suffers from extremely fast intra-band relaxation[20–22], whose interaction time-scale is typically in the range of a few ps[6]. To enhance the MEG efficiency, it is desirable to circumvent the ultrafast energy-loss intra-band process[23,24]. Recent studies suggest that the MEG is an instantaneous phenomenon occurring before the intra-band energy relaxation[25] via virtual single excitonic[26] or biexcitonic optical transition[27] or coherent superposition among multi-exciton states[12]. Other investigation suggests that the intra-band relaxation rate competes with the MEG formation rate[6].

The above mentioned photo-physical complexity of MEG is largely due to the nature of intrinsic multi-particle (or multi-exciton) interaction[28]. When more than two excitons are created under high-energy excitation condition, the lowest lying energy state is not the single exciton; the mutual interaction between two excitons results in the formation of a Coulomb-correlated two excitonic state, called biexciton[29–33]. The biexciton is energetically more stable than the single exciton such that it exists below the single-exciton state[32,34]. Recent studies have reported that the final biexciton density strongly influences the solar-conversion efficiency[25,26,35]. Although it is important to study the impact of the MEG on the transient biexciton spectra, no experimental investigations have been provided to compare the MEG-induced biexciton dynamics with the intra-band relaxation dynamics.

The key experimental observation in this study is that the optically-induced MEG is an extremely fast process, arising before the intra-band relaxation. By exploring the lowest observable biexciton dynamics, we directly measure that the biexciton bleaching comes from early emergence of the photo-induced MEG, in which the effect of extra-exciton generation is manifested by the increased broadening of the biexciton linewidth via multi-exciton interaction. Note that, in contrast to the conventional single-exciton MEG spectroscopy[11,36–39], our ultrafast time-resolved experiments were performed both in the MEG and in the non-MEG regimes via photon-energy and density-controlled measurements on the single- and biexciton spectra.

Results

Single-exciton MEG dynamics. Figure 1a shows data for the broadband optical absorption of the colloidal semiconductor PbS QDs and Fig. 1b shows a schematic for the ultrafast pump-probe measurements (See method for the detailed description of sample preparation and ultrafast spectroscopy). The lowest single-exciton bandgap energy E_x is identified as 0.93 ± 0.01 eV, and the ground-state biexciton energy E_{xx} is estimated to be 0.87 ± 0.03 eV[30–33].

Before the discussion on the biexciton dynamic, it is instructive to present detailed measurements on the intra-band relaxation dynamics because the linewidth broadening of single excitons and biexcitons is necessary related to the competing relaxation rate between the MEG and the intra-band dynamics, in which the time scale of the intra-band relaxation is typically a few ps[16,40,41], comparable with the MEG time scale. In the experiment, the colloidal semiconductor PbS QD sample was pumped by two different pump-photon energy E_{pump} with 1.55 eV and 3.10 eV, and the average number of initially photo-generated excitons per QD $\langle N_0 \rangle$, or initial exciton occupancy, was controlled from 0.1 to 2.2 to investigate the photon density-dependent E_x dynamics.

In order to determine the intra-band relaxation rate, we measured the E_x dynamics in a short Δt range between −1 ps and 7 ps as shown in Figs. 2a and b. By examining the rising edge of the E_x peak, we show that the relaxation process is completed at pump-probe delay Δt = 1 ps for $1.66E_x$ excitation (non-MEG regime) and Δt = 2 ps for $3.3E_x$ excitation (MEG regime). This 2 ps time constant is consistent with prior experimental studies of hot-carrier MEG dynamics in PbS quantum dots, where the reported value of intra-band relaxation is in the range of 2–2.5 ps[16,40,41].

Figure 2c shows the E_x transients excited by low E_{pump} (= $1.66E_x$). The observed step-like signals with a small A/B ratio (amplitude ratio of the early to late pump-probe delay Δt) are not attributed to the MEG transients, because the MEG typically requires E_{pump} greater than a few E_x. When the QDs are excited by high E_{pump} (= $3.3E_x$), we observed fast (90 ps) and slow decay (~100 ns) components with a large A/B ratio, as depicted in Fig. 2d. The experimentally determined A/B ratio of the QD occupancy was modelled via Poisson statistics (Fig. 2e)[42]. Since multiple excitons generated by the MEG decay via Auger recombination, the amplitude at long Δt (denoted by B in Fig. 2c and d) provides a scaling factor for calculating the exciton multiplicity $\langle N_x \rangle = A/B$, where A is the amplitude of single-exciton population immediately after pump excitation (denoted by A in Fig. 2c and d). By comparing the measured A/B ratios in the limit of $\langle N_0 \rangle \rightarrow 0$, a strong indication of the MEG for the $3.3E_x$ pump was identified[43]. As reported previously[16,36,38,40,44], these observations confirm that the typical MEG dynamics are observable via probing the E_x dynamics.

Transient Stark shift and biexciton linewidth broadening. The central issue to address in this paper is to investigate how the biexciton dynamics is influenced by the early formation of MEG. Figures 3a and b display the biexciton transients for the $1.66E_x$ pump and $3.3E_x$ pump as a function of Δt with controlled excitations from $\langle N_0 \rangle$ = 0.22 to $\langle N_0 \rangle$ = 2.2. Immediately after pump excitation, the photo-induced absorption (PA) exhibits rapid bleaching at E_{xx} within the first Δt = 400 fs with a much larger PA peak for the $3.3E_x$ pump than the $1.66E_x$ pump. While both signals decay non-exponentially, the signals pumped by $1.66E_x$ decay to zero after a few ps, and the transients pumped by $3.3E_x$ change their signs from positive to negative near Δt = 2 ps.

In a strong quantum-confinement regime, the pump-created local electric field induces a large transient shift of absorption, a phenomenon known as transient Stark shift[42,45]. This effect is more considerable with increasing photo-generated carriers, which in turn produces a stronger local field and complicates the ultrafast PA spectra as schematically shown in Fig. 3c. Note that the increased carrier density is reflected both by the carrier-induced Stark shift and by the absorption linewidth Γ that leads to a broader feature[46,47]. As discussed later, this broadened Γ directly determines the effect of MEG on the biexciton dynamics through extra-exciton generation.

It is expected that high E_{pump} excitation, larger than E_x, enhances the Γ broadening due to the extra-exciton generation. Immediately after the pump (Δt = 400 fs), we clearly observe that the biexciton Γ is broader for the $3.3E_x$ excitation case than for the $1.66E_x$ one, as shown in Figs. 3d and e with two different excitations of $\langle N_0 \rangle$ for each E_{pump} excitation. Thus, the observed transient PA dynamics can be understood by combined effects of both the carrier-induced transient

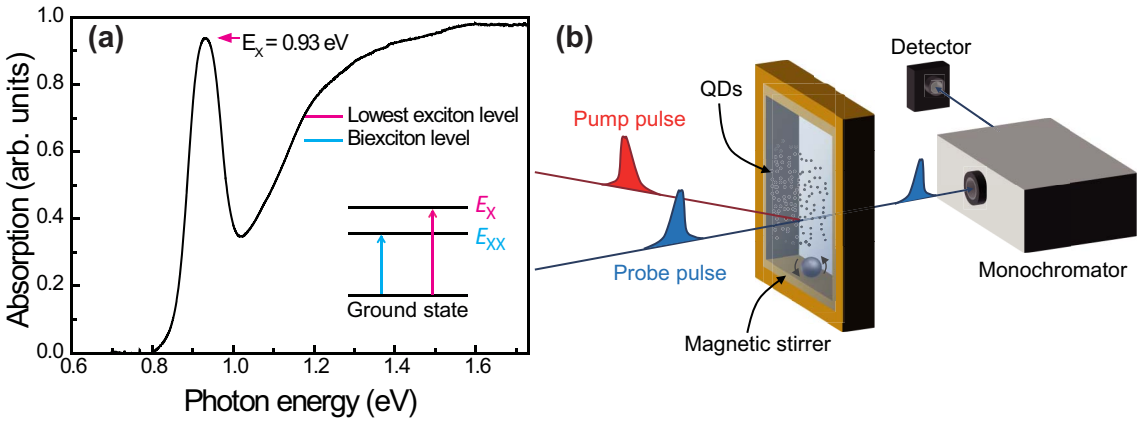

Figure 1 | QD absorption spectra and experimental setup. (a) Linear absorption spectra of the colloidal PbS QDs used in the study. Inset: schematic energy levels for the single-exciton E_x and the ground-state biexciton E_{xx}, respectively. (b) Schematic for the ultrafast pump-probe measurements. For the spectrally-resolved measurements, the probe pulse is scanned through a monochromator (Newport 74125 Oriel Cornerstone 260 1/4 m) at each Δt. The measured FWHM of the pump and probe beam are 150 μm and 100 μm, respectively. All measurements are performed at room temperature.

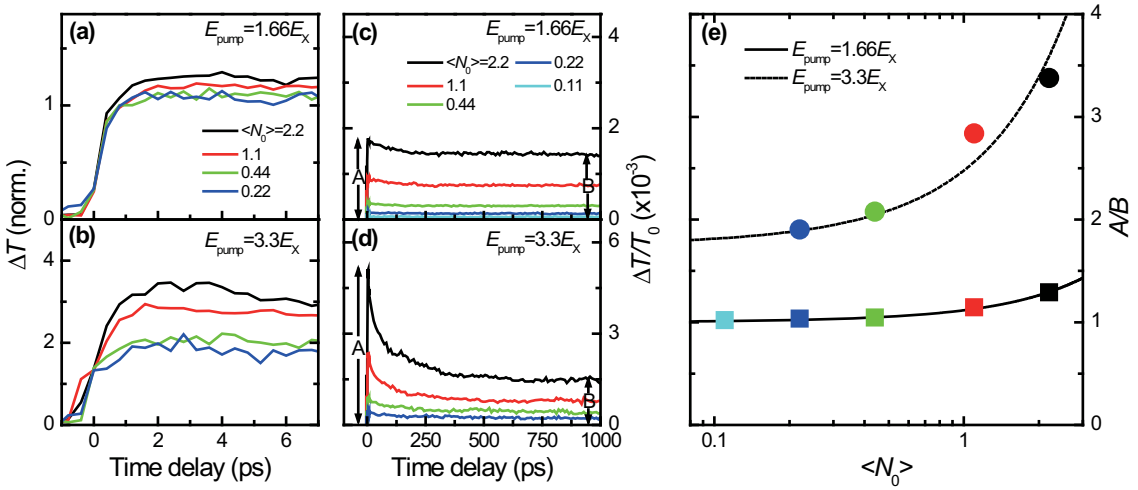

Figure 2 | Single-exciton MEG dynamics. Single-exciton dynamics in a short pump-probe range between −1 and 7 ps for 1.66E_x (a) and 3.3E_x excitations (b). The differential transmission signals probed at E_x with the 1.66E_x pump (c) and the 3.3E_x pump (d) are displayed with $\langle N_0 \rangle$ ranging from 0.11 to 2.2. Here, $\langle N_0 \rangle$ is estimated via $\langle N_0 \rangle = j_p \sigma_a$, where j_p is the pump fluence in unit of photons per cm^2 and σ_a is the absorption cross-section in unit of cm^2 [14]. (c) The experimentally measured A/B ratio is shown for the 1.66E_x pump (filled circle) and for the 3.3E_x pump (filled square). The calculated A/B ratio is obtained via Poisson distribution of the QD occupancies for the 1.66E_x pump (solid line) and for the 3.3E_x pump (dashed line).

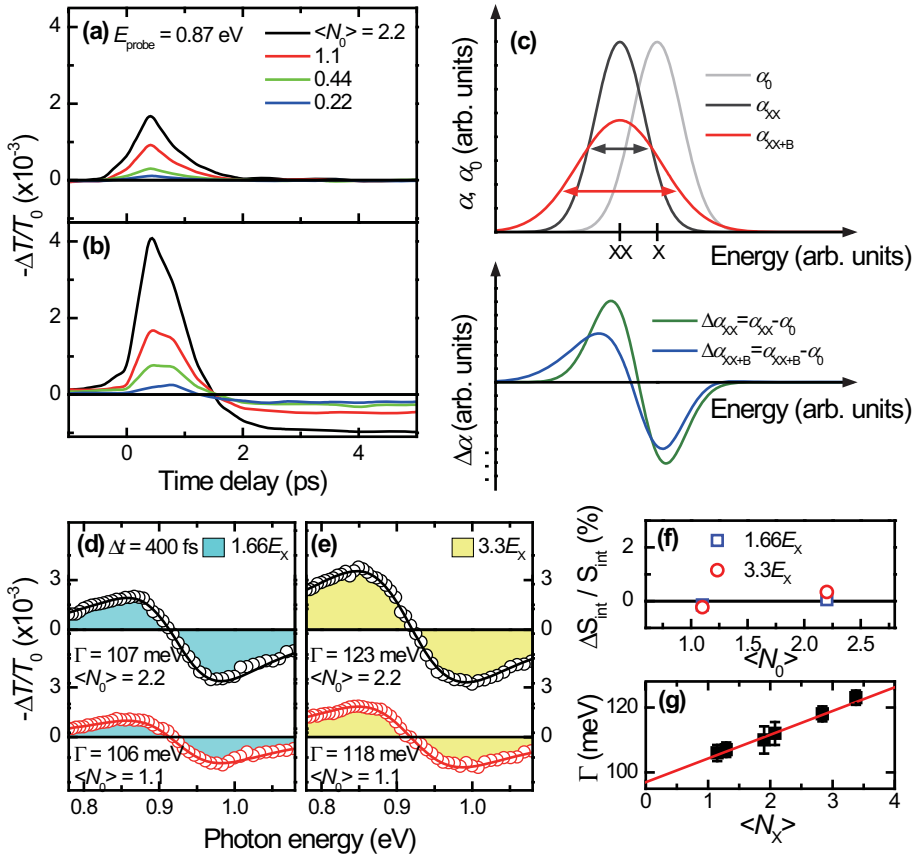

Figure 3 | Ultrafast MEG-induced biexciton transients before the intra-band relaxation. Transient E_{xx} dynamics are shown as a function of Δt for the 1.66E_x pump (a) and for the 3.3E_x pump (b) with various $\langle N_0 \rangle$. (c) Schematic illustration of the PA caused by the transient Stark shift of the single-exciton absorption (black line) and the corresponding photo-induced biexciton broadening (red line). The gray line indicates the single-exciton absorption without the pump. The differential PA spectra exhibit an energy-shifted broader feature (blue line) due to the MEG-induced exciton scattering compared to the case of no MEG (green line). The spectrally-resolved PA spectra with the probe range from 0.78 to 1.08 eV measured at Δt = 400 fs are shown for the 1.66E_x pump (d) and for the 3.3E_x pump (e) with two different $\langle N_0 \rangle$. Solid lines represent numerical fits using equation (1). The obtained biexciton Γ for the 1.66E_x pump with $\langle N_0 \rangle$ = 1.1 and 2.2 are 106 meV and 107 meV, respectively, and those for the 3.3E_x pump with $\langle N_0 \rangle$ = 1.1 and 2.2 are 118 meV and 123 meV, respectively. (f) Spectrally integrated areas of the broadened biexciton absorption. (g) The biexciton Γ broadening linearly increases with increasing the total number of excitons. The experimentally determined Γ (black filled squares) from the Figs. 3d and e are compared to the equation (2).

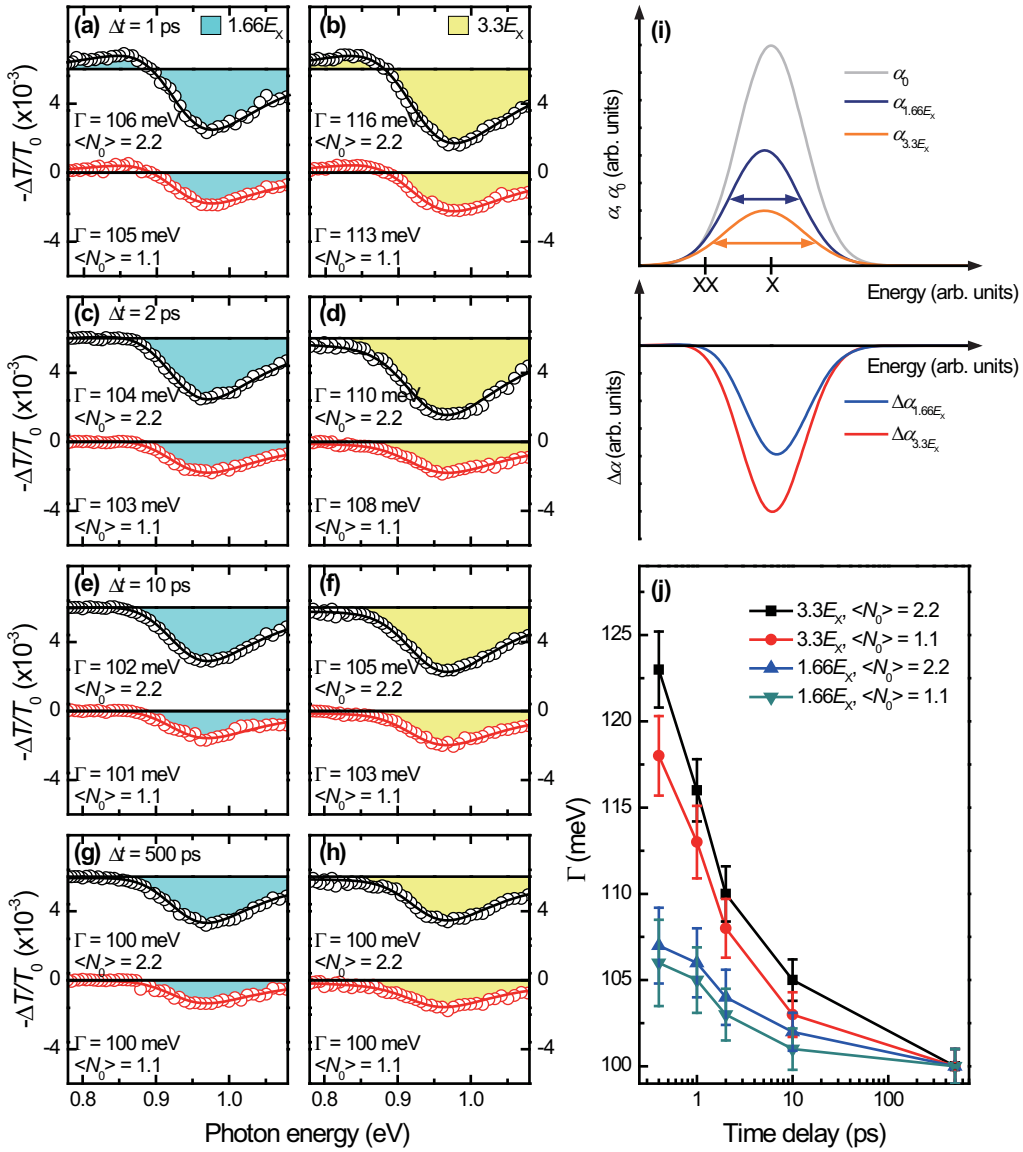

Figure 4 | Biexciton broadening at longer delays than 400 fs. The single- and biexciton absorption change spectra at Δt of 1 ps (a,b), 2 ps (c,d), 10 ps (e,f) and 500 ps (g,h) with two E_{pump}. (i) Schematic illustration of the PA bleaching dynamics at longer $\Delta t > 2$ ps for the $1.66E_x$ pump (blue line) and for the $3.3E_x$ pump (orange line). (j) Transient Γ broadening is shown as function of Δt.

Stark shift and the MEG-induced biexciton Γ broadening. We additionally notice that the spectrally-integrated areas of the broadened biexciton absorption remain the same regardless of $\langle N_0 \rangle$ as shown Fig. 3f. This constraint indicates that the broadening is determined by the number of excitons, and it ensures that the biexciton PA peak is reduced by the exciton-exciton collision-induced broadening rather than the phase-space filling argument[46].

Quantitative analysis of the MEG-induced biexciton broadening and the early emergence of MEG. The entire pump-induced changes of the absorption spectra can be faithfully fit via the following third-order susceptibility function[31,33],

$$\Delta\alpha \propto \Im\left(\chi^{(3)}(\omega)\right) = \Im\left(|E_L|^2\left(-\frac{\mu_X^4}{\hbar\omega - E_X + i\Gamma} + \frac{\mu_{XX}^4}{\hbar\omega - E_X + \Delta_{XX} + i\Gamma}\right)\right), \quad (1)$$

where E_L is the electric field of the pump, Δ_{XX} is the biexciton binding energy, and μ_X and μ_{XX} are the transition dipole moments from the ground state to E_x and to E_{xx}, respectively. The first term represents the bleaching at E_x and the second term represents the PA at ground-state E_{xx}. For the PA dynamics measured at Δt = 400 fs (Figs. 3d and e), because the intra-band relaxation time (2 ps) is longer than Δt of 400 fs, the absorption change measured at E_x was not induced by the single-exciton state filling. In addition, Auger recombination and impact ionization (Auger processes) can be neglected because the time-scale of Auger processes is much slower (100 ~ 200 ps) than the intra-band relaxation. On the other hand, the difference in Γ, obtained from a fit of equation (1) to the measured PA spectra, shows that the broadening is associated with the MEG-induced biexciton broadening.

For quantitative analysis, the biexciton Γ is plotted as a function of the average number of total excitons per QD $\langle N_x \rangle$, and the results are displayed in Fig. 3g. Here, we note that the definition of $\langle N_x \rangle$ (obtained from the measured A/B ratios in Fig. 2c) differs from that of $\langle N_0 \rangle$ in a sense that $\langle N_x \rangle$ includes both the average number of initially photo-generated excitons and the MEG-induced excitons per QD; $\langle N_0 \rangle$ is the average number of photo-generated exciton per QD[11]. In other words, the biexciton broadening is directly related

to the total number of excitons $\langle N_x \rangle$, not by the initial exciton occupancy $\langle N_0 \rangle$. By plotting the Γ as a function of $\langle N_x \rangle$, we obtain a linear relationship of

$$\Gamma(N_x) = \Gamma(0) + \gamma N_x, \quad (2)$$

where γ (= 6.8 meV per exciton) is the Γ broadening parameter per exciton. Because $\Gamma(0)$ represents the linewidth broadening in the absence of photo-generated excitons, the value should corresponds to the E_x broadening in Fig. 1a. A simple Gaussian fit shows that the E_x broadening in Fig. 1a is 100 ± 5 meV, well corroborated with the fitted $\Gamma(0)$ = 98 meV of the biexciton broadening. The characteristic broadening of Γ with increasing $\langle N_x \rangle$ entails the effect of MEG, i.e. as more excitons are injected, more broaden feature of biexciton Γ is expected.

Discussion

The early emergence of the MEG is substantiated by measuring the single- and biexciton spectra before/after the intra-band relaxation of 2 ps. It is expected that Γ should be large if Δt is shorter than the intra-band relaxation time, i.e. if the MEG-induces exciton-exciton scattering occurs earlier than the intra-band relaxation, Γ before the intra-band relaxation is larger than Γ after intra-band relaxation. Figures 4 (a) and (b) show the PA signals at Δt = 1 ps. As expected, the Γ broadening at Δt = 1 ps is smaller than at Δt = 400 fs, but larger than at Δt = 2 ps. Figures 4c and d show the spectra at Δt = 2 ps for the $1.66E_x$ pump and for the $3.3E_x$ pump, respectively. The Γ at 2 ps for $3.3E_x$ with $\langle N_0 \rangle$ = 2.2 is 110 meV while the Γ at Δt = 400 fs with same condition is 123 meV. Indeed, we clearly see that Γ at Δt = 2 ps is smaller than that of before intra-band relaxation both for the two $\langle N_0 \rangle$ excitations (see Fig. 3e and Figs. 4b and d).

Long after the intra-band relaxation finishes, the carrier-induced Stark shift becomes weak, and the single-exciton state filling is dominant (Figs. 4e–h). As schematically shown in Fig. 4i, the weak Stark shift is rendered as the absence of PA signals at 0.85 eV, but the effect is not completely vanished; negative PA peaks appear at 0.97 eV instead of the single-exciton energy of 0.93 eV in Fig. 1a. Because the PA peak is proportional to the generated exciton numbers, the magnitude of bleaching is larger for the case of $3.3E_x$ pump than the $1.66E_x$ pump case. We note that the chosen two E_{pump} ($1.66E_x$ and $3.3E_x$) set the below and upper limit on the occurrence of MEG such that the observed two dynamics (before and after the intra-band relaxation) are distinguishable in comparing the MEG-induced biexciton lineshape and the single-exciton-dominated one. There is a possibility that significant re-shaping of single-exciton spectra can be observed at longer Δt, which may occur when as many as 50% of QDs are occupied by multiple electron-hole pairs (i.e. $\langle N_0 \rangle < 1$). This scenario can be excluded in our investigation because the PA peaks at Δt = 2 ps show negligible energy shifts[48] even when $\langle N_0 \rangle > 1$.

To investigate the effect of Auger and single-exciton recombination on Γ, we compare the PA spectra at Δt of 10 ps and 500 ps. We noted that the single-exciton decay dynamics consists of two relaxation components (see Figs. 2c and d): one is "fast" Auger recombination (known as biexcitonic relaxation component[6]) and another is "slow" single-exciton recombination (referred to as excitonic background[6]). Figures 4e and f display the PA spectra at Δt = 10 ps. Because the Auger recombination is not completed, Γ at Δt = 10 ps is smaller than Γ at Δt = 2 ps. After the Auger recombination is finished, $\langle N_x \rangle$ at Δt = 500 ps approaches one both for the $1.66E_x$ and $3.3E_x$ pump cases. Because nearly one exciton is left at Δt = 500 ps, Γ for both E_{pump} (Figs. 4g and h) is identical with Γ of 100 meV, representing negligible effect of single-exciton recombination on Γ.

The measured data are summarized in Fig. 4j. Two main aspects are addressed. First, Γ at Δt = 400 fs is the largest compared to the Γ at $\Delta t > 400$ fs, providing an evidence for the large biexciton Γ broadening in early Δt. Second, by observing the fact that the decreasing slope of Γ with Δt for $3.33E_x$ excitation is steeper than the $1.66E_x$ excitation up to Δt = 2 ps, we can find that the effect of MEG on Γ is strongly influenced by extra-exciton generation before the intra-band relaxation.

To conclude, we have investigated the transient dynamics of biexciton, located below the single-exciton energy, and have explored the impact of MEG on the biexciton spectra. Our ultrafast spectroscopy shows that the linewidth broadening of the biexciton spectra provides direct evidence on the early emergence of the MEG compared to the intra-band relaxation time. We additionally have presented quantitative analysis that the broadening parameter Γ per exciton increases linearly with increasing the total number of excitons. For detailed time-resolved spectral analysis, the PA spectra are compared with single-exciton ones at Δt = 400 fs and longer delays. The comparison underscores that Γ broadening before Δt = 2 ps is larger than the Γ after Δt = 2 ps, corroborating that the MEG indeed occurs before the intra-band relaxation.

Methods

Synthesis of PbS quantum dots. Our PbS colloidal quantum dots are capped using eleic acid and dispersed in toluene. The synthesis of the sample followed a procedure that used standard air-free solution based technique[49]. In a typical synthesis, 2.0 mmol of PbO (0.445 g), 8.0 mmol (2.25 g) of oleic acid (OA), and 9.9 mmol (2.5 g) of 1-octadecene (ODE) are placed in a flask and heated to 100°C under vacuum, and then nitrogen was introduced. The temperature was controlled to the appropriate injection temperature (100 to 150°C) to obtain the desired particle size. The sulfur precursor was prepared by mixing bis(trimethylsilyl)sulfide with ODE. Removal of excess ligand was completed by repeated the followings: precipitation in acetone, centrifugation of the particles, and dispersion in toluene.

PbS QDs and ultrafast spectroscopy. The sample used in this experiment is semiconductor colloidal PbS QDs dispersed in toluene with an average diameter of approximately 5.1 nm. The broadband optical absorption is measured by a Fourier transform infrared (FTIR) spectrometer (Bomem DA8). For the ultrafast pump-probe spectroscopy, the colloidal PbS QDs are maintained in a 3-mm cell contained in the toluene liquid with two optically-transparent MgO windows, and the samples are actively stirred using a magnetic stirrer to ensure that photo-charging does not occur during the measurements (Fig. 1b)[50]. Using a 250 kHz Ti-sapphire regenerative amplifier (Coherent RegA 9050), the samples are excited by 50 fs pulses with a pump-photon energy E_{pump} of 1.55 eV and its second harmonic E_{pump} of 3.10 eV for investigating the MEG photo-dynamics. A fraction of the amplifier output is used as a probe pulse with photon energy E_{probe} of 0.93 eV for the lowest E_x and 0.87 eV for the E_{xx}. Both probe pulses are delivered from wavelength-tunable optical parametric amplifier (Coherent OPA 9850).

1. Shockley, W. & Queisser, H. J. Detailed Balance Limit of Efficiency of p-n Junction Solar Cells. *J. Appl. Phys.* **32**, 510–519 (1961).
2. Yu, G., Gao, J., Hummelen, J. C., Wudl, F. & Heeger, A. J. Polymer Photovoltaic Cells: Enhanced Efficiencies via a Network of Internal Donor-Acceptor Heterojunctions. *Science* **270**, 1789–1791 (1995).
3. Semonin, O. E. *et al.* Peak external photocurrent quantum efficiency exceeding 100% via MEG in a quantum dot solar cell. *Science* **334**, 1530–1533 (2011).
4. Trinh, M. T. *et al.* Direct generation of multiple excitons in adjacent silicon nanocrystals revealed by induced absorption. *Nat. Photonics* **6**, 316–321 (2012).
5. Timmerman, D., Valenta, J., Dohnalová, K., de Boer, W. D. A. M. & Gregorkiewicz, T. Step-like enhancement of luminescence quantum yield of silicon nanocrystals. *Nat. Nanotechnol.* **6**, 710–713 (2011).
6. Schaller, R. D. & Klimov, V. I. High Efficiency Carrier Multiplication in PbSe Nanocrystals: Implications for Solar Energy Conversion. *Phys. Rev. Lett.* **92**, 186601 (2004).
7. Nozik, A. J. Multiple exciton generation in semiconductor quantum dots. *Chem. Phys. Lett.* **457**, 3–11 (2008).
8. Wolf, M., Brendel, R., Werner, J. H. & Queisser, H. J. Solar cell efficiency and carrier multiplication in $Si_{1-x}Ge_x$ alloys. *J. Appl. Phys.* **83**, 4213–4221 (1998).
9. De Boer, W. D. A. M. *et al.* Red spectral shift and enhanced quantum efficiency in phonon-free photoluminescence from silicon nanocrystals. *Nat. Nanotechnol.* **5**, 878–884 (2010).
10. Unold, T., Mueller, K., Lienau, C., Elsaesser, T. & Wieck, A. Optical Control of Excitons in a Pair of Quantum Dots Coupled by the Dipole-Dipole Interaction. *Phys. Rev. Lett.* **94**, 137404 (2005).
11. Schaller, R. D., Sykora, M., Pietryga, J. M. & Klimov, V. I. Seven excitons at a cost of one: redefining the limits for conversion efficiency of photons into charge carriers. *Nano Lett.* **6**, 424–429 (2006).
12. Ellingson, R. J. *et al.* Highly efficient multiple exciton generation in colloidal PbSe and PbS quantum dots. *Nano Lett.* **5**, 865–871 (2005).

13. Nozik, A. J. Exciton multiplication and relaxation dynamics in quantum dots: applications to ultrahigh-efficiency solar photon conversion. *Inorg. Chem.* **44**, 6893–6899 (2005).
14. Moreels, I. *et al.* Size-dependent optical properties of colloidal PbS quantum dots. *ACS Nano* **3**, 3023–3030 (2009).
15. Korkusinski, M., Voznyy, O. & Hawrylak, P. Fine structure and size dependence of exciton and biexciton optical spectra in CdSe nanocrystals. *Phys. Rev. B* **82**, 245304 (2010).
16. Nootz, G. *et al.* Size dependence of carrier dynamics and carrier multiplication in PbS quantum dots. *Phys. Rev. B* **83**, 155302 (2011).
17. Timmerman, D., Izeddin, I., Stallinga, P., Yassievich, I. N. & Gregorkiewicz, T. Space-separated quantum cutting with silicon nanocrystals for photovoltaic applications. *Nat. Photonics* **2**, 105–109 (2008).
18. Nozik, A. J. Nanoscience and nanostructures for photovoltaics and solar fuels. *Nano Lett.* **10**, 2735–2741 (2010).
19. Klimov, V. I. Spectral and dynamical properties of multiexcitons in semiconductor nanocrystals. *Annu. Rev. Phys. Chem.* **58**, 635–73 (2007).
20. Sosnowski, T. S. *et al.* Rapid carrier relaxation in $In_{0.4}Ga_{0.6}As$/GaAs quantum dots characterized by differential transmission spectroscopy. *Phys. Rev. B* **57**, R9423–R9426 (1998).
21. Nair, G., Chang, L.-Y., Geyer, S. M. & Bawendi, M. G. Perspective on the prospects of a carrier multiplication nanocrystal solar cell. *Nano Lett.* **11**, 2145–2151 (2011).
22. Kambhampati, P. Hot Exciton Relaxation Dynamics in Semiconductor Quantum Dots: Radiationless Transitions on the Nanoscale. *J. Phys. Chem. C* **115**, 22089–22109 (2011).
23. Urayama, J., Norris, T., Singh, J. & Bhattacharya, P. Observation of Phonon Bottleneck in Quantum Dot Electronic Relaxation. *Phys. Rev. Lett.* **86**, 4930–4933 (2001).
24. Miaja-Avila, L. *et al.* Direct mapping of hot-electron relaxation and multiplication dynamics in PbSe quantum dots. *Nano Lett.* **12**, 1588–1591 (2012).
25. Franceschetti, A., An, J. M. & Zunger, A. Impact ionization can explain carrier multiplication in PbSe quantum dots. *Nano Lett.* **6**, 2191–2195 (2006).
26. Schaller, R. D., Agranovich, V. M. & Klimov, V. I. High-efficiency carrier multiplication through direct photogeneration of multi-excitons via virtual single-exciton states. *Nat. Phys.* **1**, 189–194 (2005).
27. Rupasov, V. & Klimov, V. I. Carrier multiplication in semiconductor nanocrystals via intraband optical transitions involving virtual biexciton states. *Phys. Rev. B* **76**, 125321 (2007).
28. Klimov, V., Hunsche, S. & Kurz, H. Biexciton effects in femtosecond nonlinear transmission of semiconductor quantum dots. *Phys. Rev. B* **50**, 8110–8113 (1994).
29. Kim, K., Norris, T. B. & Hohenester, U. Redshift of the excited state due to a nondegenerate biexciton in self-organized quantum dots. *J. Appl. Phys.* **103**, 113702 (2008).
30. Hu, Y., Koch, S. & Lindberg, M. Biexcitons in semiconductor quantum dots. *Phys. Rev. Lett.* **64**, 1805–1807 (1990).
31. Banyai, L., Hu, Y., Lindberg, M. & Koch, S. Third-order optical nonlinearities in semiconductor microstructures. *Phys. Rev. B* **38**, 8142–8153 (1988).
32. Banyai, L. Asymptotic biexciton "binding energy" in quantum dots. *Phys. Rev. B* **39**, 8022–8024 (1989).
33. Hu, Y., Lindberg, M. & Koch, S. Theory of optically excited intrinsic semiconductor quantum dots. *Phys. Rev. B* **42**, 1713–1723 (1990).
34. Sewall, S., Franceschetti, A., Cooney, R., Zunger, A. & Kambhampati, P. Direct observation of the structure of band-edge biexcitons in colloidal semiconductor CdSe quantum dots. *Phys. Rev. B* **80**, 081310 (2009).
35. Shabaev, A., Efros, A. L. & Nozik, A. J. Multiexciton generation by a single photon in nanocrystals. *Nano Lett.* **6**, 2856–63 (2006).
36. Stewart, J. T. *et al.* Comparison of carrier multiplication yields in PbS and PbSe nanocrystals: the role of competing energy-loss processes. *Nano Lett.* **12**, 622–628 (2012).
37. Nair, G., Geyer, S., Chang, L.-Y. & Bawendi, M. Carrier multiplication yields in PbS and PbSe nanocrystals measured by transient photoluminescence. *Phys. Rev. B* **78**, 125325 (2008).
38. Beard, M. C. *et al.* Multiple exciton generation in colloidal silicon nanocrystals. *Nano Lett.* **7**, 2506–2512 (2007).
39. Schaller, R. D., Pietryga, J. M. & Klimov, V. I. Carrier multiplication in InAs nanocrystal quantum dots with an onset defined by the energy conservation limit. *Nano Lett.* **7**, 3469–3476 (2007).
40. Gesuele, F. *et al.* Ultrafast Supercontinuum Spectroscopy of Carrier Multiplication and Biexcitonic Effects in Excited States of PbS Quantum Dots. *Nano Lett.* **12**, 2658–2664 (2012).
41. Istrate, E. *et al.* Carrier relaxation dynamics in lead sulfide colloidal quantum dots. *J. Phys. Chem. B* **112**, 2757–2560 (2008).
42. Klimov, V. I. Optical nonlinearities and ultrafast carrier dynamics in semiconductor nanocrystals. *J. Phys. Chem. B* **104**, 6112–6123 (2000).
43. Schaller, R. & Klimov, V. Non-Poissonian Exciton Populations in Semiconductor Nanocrystals via Carrier Multiplication. *Phys. Rev. Lett.* **96**, 097402 (2006).
44. McGuire, J. A., Joo, J., Pietryga, J. M., Schaller, R. D. & Klimov, V. I. New aspects of carrier multiplication in semiconductor nanocrystals. *Acc. Chem. Res.* **41**, 1810–1819 (2008).
45. Cho, B., Peters, W. K., Hill, R. J., Courtney, T. L. & Jonas, D. M. Bulklike hot carrier dynamics in lead sulfide quantum dots. *Nano Lett.* **10**, 2498–2505 (2010).
46. Wake, D., Yoon, H., Wolfe, J. & Morkoc, H. Response of excitonic absorption spectra to photoexcited carriers in GaAs quantum wells. *Phys. Rev. B* **46**, 13452–13460 (1992).
47. Honold, A., Schultheis, L., Kuhl, J. & Tu, C. W. Collision broadening of two-dimensional excitons in a GaAs single quantum well. *Phys. Rev. B* **40**, 6442–6445 (1989).
48. Malko, A. V., Mikhailovsky, A. A., Petruska, M. A., Hollingsworth, J. A. & Klimov, V. I. Interplay between Optical Gain and Photoinduced Absorption in CdSe Nanocrystals. *J. Phys. Chem. B* **108**, 5250–5255 (2004).
49. Hines, M. A. & Scholes, G. D. Colloidal PbS Nanocrystals with Size-Tunable Near-Infrared Emission: Observation of Post-Synthesis Self-Narrowing of the Particle Size Distribution. *Adv. Mater.* **15**, 1844–1849 (2003).
50. McGuire, J. A., Sykora, M., Joo, J., Pietryga, J. M. & Klimov, V. I. Apparent versus true carrier multiplication yields in semiconductor nanocrystals. *Nano Lett.* **10**, 2049–2057 (2010).

Acknowledgments

The work at Yonsei was supported by the National Research Foundation of Korea (NRF) grant funded by the Korea government (MSIP) (NRF-2011-0013255, NRF-2011-220-D00052, NRF-2011-0028594, NRF-2009-0083512, NRF-2012R1A1A2043180) and the LG Display Academic Industrial Cooperation Program. S. C. Lim and Y. H. Lee at SKKU are grateful for the support by Institute for Basic Science (grant number EM 1304).

Author contributions

H.C. and Y.H.L. developed the original experimental ideas. Y.C. and S.S. performed the ultrafast pump-probe measurements. Y.C. and S.C.L. prepared the colloidal QD samples and analyzed the data. The manuscript was written through contributions of all authors.

Additional information

Competing financial interests: The authors declare no competing financial interests.

How to cite this article: Choi, Y., Sim, S.W., Lim, S.C., Lee, Y.H. & Choi, H.Y. Ultrafast biexciton spectroscopy in semiconductor quantum dots: evidence for early emergence of multiple-exciton generation. *Sci. Rep.* **3**, 3206; DOI:10.1038/srep03206 (2013).